Journal of Macromolecular Science, Part A
Publication details, including instructions for authors and subscription information:
http://www.informaworld.com/smpp/title~content=t713597274

Synthesis, Characterization and Electrorheological Properties of Polyaniline/Titanate Core-Shell Composite

Lijun Ji[a]; Jiexu Zhang[a]
[a] College of Chemical Engineering, East China University of Science and Technology, Shanghai, China

To cite this Article Ji, Lijun and Zhang, Jiexu(2009) 'Synthesis, Characterization and Electrorheological Properties of Polyaniline/Titanate Core-Shell Composite', Journal of Macromolecular Science, Part A, 46: 7, 688 — 693
To link to this Article: DOI: 10.1080/10601320902938988
URL: http://dx.doi.org/10.1080/10601320902938988

Journal of Macromolecular Science®, Part A: Pure and Applied Chemistry (2009) **46**, 688–693

ISSN: 1060-1325 print / 1520-5738 online
DOI: 10.1080/10601320902938988

Taylor & Francis
Taylor & Francis Group

Synthesis, Characterization and Electrorheological Properties of Polyaniline/Titanate Core-Shell Composite

LIJUN JI* and JIEXU ZHANG

College of Chemical Engineering, East China University of Science and Technology, 200237 Shanghai, China

Received November 2008, Accepted January 2009

In this study, a facile method was developed for the preparation of a new conducting polymer composite with core-shell structure. The surfaces of layered titanate ($K_2Ti_4O_9$) particles were first modified with 3-aminopropyltriethoxysilane, and then a polyaniline/titanate (PANI/$K_2Ti_4O_9$) composite was synthesized via chemical oxidative polymerization. The resulting composites were characterized by SEM, XRD, FTIR and TG measurements. The results indicated that the PANI deposited on the surface of $K_2Ti_4O_9$ particles resulted in the formation of the composite with a core-shell structure. TG analysis showed that the composite containing 28.7 wt% PANI had better thermal stability than that of pure PANI. Further, the PANI/$K_2Ti_4O_9$ composite particles were adopted as a dispersed phase in silicone oil for electrorheological (ER) investigation. Suspension of the composite particles exhibited typical ER behavior subjected to an external electric field under steady and dynamic oscillatory shear.

Keywords: Polyaniline, layered titanate, composite, electrorheological fluid, viscoelasticity

1 Introduction

Synthesis of composite materials is an effective approach to combine the features of different materials and tailor the properties to produce the desired material with superior performance (1). In this regard, composites based on conducting polymers have been extensively explored during the last several decades due to their excellent chemical and physical properties arising from their unique π-conjugated system (2). In particular, encapsulation of inorganic particles inside the shell of conducting polymers is the most popular and interesting aspect of composite synthesis in recent years. So far, a number of studies have been reported on the encapsulation of metal, oxide, sulfide, carbon nanotubes and clay particles into the shell of conducting polymers. The resulting composites exhibit enhanced solubility, conductivity, magnetic, optoelectronic and electrorheological (ER) properties (3–8).

On the other hand, ER fluids, as one of the most important smart materials, have also attracted much attention because of their interesting rheological properties under an external electric field. A typical ER fluid consists of dielectric particles dispersed in an insulating liquid medium. Upon application of an electric field, the dispersed dielectric particles will be polarized and attracted to each other to form a chain or column structure (9,10). These chains and columns enable the ER fluid to undergo a rapid transition from Newtonian liquid to rigid solid and its rheological properties (i.e., shear stress, viscosity and viscoelasticity) can be dramatically and reversibly changed with a strong electric field, which provides ER fluids with potential applications in mechanical devices such as clutches, dampers, brakes (11). To further improve the ER performance of ER fluids, various anhydrous ER materials have been explored (12–18). Among them, conducting polymer/inorganic composites have the advantage of materials with a good ER efficiency (19–22).

Among all the inorganic particles, layered alkali titanates are generally considered to be one of the most important inorganic materials as they have potential applications in the fields of photocatalysis, photoluminescence, fuel cell electrolytes and chemical sensors. Hence, encapsulation of titanates into conducting polymers may provide materials with different photoelectric characteristics. Meanwhile, due to their inherent chemical structure which consists of high-dielectric constant titanate layers intercalated with alkali-ions, the local shift of alkali-ions loosely bounded in layers might enhance the available polarization for good ER effect under electric field (23). Therefore, conducting polymer combined with titanates might give rise to interesting ER behavior. Although some papers concerning conducing polymers/TiO_2 (19,24) have been published, few studies

*Address correspondence to: Lijun Li, College of Chemical Engineering, East China University of Science and Technology, 200237 Shanghai, China. Tel: +86-21-64253914; Fax: +86-21-64253914; E-mail: jilijun@ecust.edu.cn

dealing with alkali titanates encapsulated into conducting polymers have been reported (25,26).

In this work, we synthesized a new core-shell composite of PANI/$K_2Ti_4O_9$ via surface polymerization, where the surface of $K_2Ti_4O_9$ particles was modified by 3-aminopropyltriethoxysilane in advance and then anilinium ions bonded on the tail of silane were polymerized. PANI is one of the most promising conducting polymers with high polarizability, conductivity, environmental stability and good ER properties. The morphology and structure of the composite were characterized by different experimental techniques. The ER properties of PANI/$K_2Ti_4O_9$ composite based fluid under steady and dynamic oscillatory shear were also investigated.

2 Experimental

2.1 Materials

Aniline (Aldrich, 99%) was distilled under reduced pressure before use. Ammonium persulfate (APS, $(NH4)_2S_2O_8$, 98%) and 3-aminopropyltriethoxysilane were purchased from Aldrich Chemicals Co., and other high-purity chemicals were used as received.

2.2 Surface Modification of $K_2Ti_4O_9$

The layered material $K_2Ti_4O_9$ was prepared by a conventional solid-state reaction between K_2CO_3 and TiO_2 powders in a 1:3.5 molar ratio. The mixture was calcined at 800°C in air for 20 h (27).

The resulting $K_2Ti_4O_9$ powder was then modified with 3-aminopropyltriethoxysilane. The process can be described as follows: 1 mL of 3-aminopropyltriethoxysilane was dissolved in 100 mL toluene. Then, 2.0 g of titanate was added into the above solution and stirred vigorously. After flowing N_2 through the mixture for 10 min, the solution was refluxed at 80°C for 6 h. Finally, the product was washed with acetone and distilled water, and then dried in a vacuum oven at 80°C for 6 h.

2.3 Synthesis of PANI/ $K_2Ti_4O_9$ Core-Shell Composite

In a typical synthesis, 2.0 g of silane-modified titanate was dispersed in 100 mL distilled water under ultrasonic condition for 0.5 h. 1.0 mL aniline monomer was then added to the above solution. The mixture was stirred vigorously at 0–5°C. Pre-cooled ammonium persulfate (APS) solution (the molar ratio of APS to aniline was 1.25) was introduced into the mixture dropwise with vigorous stirring, and the polymerization was allowed to proceed for 24 h at 0–5°C. Finally, the product was filtered and washed with methanol and distilled water, and then dried *in vacuo* at 80°C for 12 h.

2.4 Characterization of Materials

X-ray diffraction patterns were determined with Rigaku D/MAX 2550V diffractometer using Cu Kα radiation (λ = 1.5406 Å). FT-IR spectra of the samples were obtained on Nicolet Magna-550 spectrometer in the range of 4000–400 cm^{-1}.Thermogravimetric analysis (TGA) was carried out with a TGA/SDTA 851^e at a heating rate of 10°C/min in air. The morphology of the nanocomposite was studied using JEOL JSM-6360LV scanning electron microscope (SEM).

2.5 Preparation of ER Fluids and ER Measurements

For the preparation of the suspensions, PANI/$K_2Ti_4O_9$ particles were first dedoped by immersion in 3 vol% aqueous ammonia and then dried in a vacuum oven at 70°C for 12 h. The dried particles were dispersed in silicone oil (Fluid 200, Dow Corning, UK; viscosity η_c = 108 mPa·s, density d_c = 0.965 g/cm^3) to form the fluid concentration of 5% (v/v).

Measurements of rheological properties of the prepared fluids were carried out under controlled shear-rate and shear-stress mode using a coaxial cylinder viscometer (Bohlin GEMINI, Malvern Instruments, UK). The suspensions were placed in the Couette cell with the rotating inner cylinder of 14 mm diameter and the outer cylinder separated by a 0.7 mm gap. They were connected to a DC power supply producing a field strength E = 0.5–3 kV mm^{-1}. Further, dynamic viscoelastic tests were performed by dynamic strain sweeps and frequency sweeps. The strain sweep was carried out with applied strains of 10^{-4} to 1.0 at a frequency of 62.8 rad/s under an electric field to determine the linear viscoelastic region. The rheological parameters were then obtained from the frequency sweep tests (0.62 to 314 rad/s) at a fixed strain amplitude in the linear viscoelastic region.

3 Results and discussion

3.1 Material Characteristics

Figure 1 shows typical SEM images of prepared $K_2Ti_4O_9$ and PANI/$K_2Ti_4O_9$ composite. The layered $K_2Ti_4O_9$ (Figure 1a) shows the flat surfaces with different lengths of edges, while PANI/$K_2Ti_4O_9$ particles have a rougher surface and salient morphology change occurs on the external surface of the composite particles, which is due to the PANI deposited on the surface (Figure 1b). The silane-modified $K_2Ti_4O_9$ particles exhibit hydrophobic behavior because of the hydrophobic $-NH_2$ group. As the hydrophobic aniline monomers are added into the solution of silane-modified $K_2Ti_4O_9$, the monomers are preferably adsorbed onto the surface of the $K_2Ti_4O_9$ particles through hydrophobic-hydrophobic interaction. Therefore, the ani-

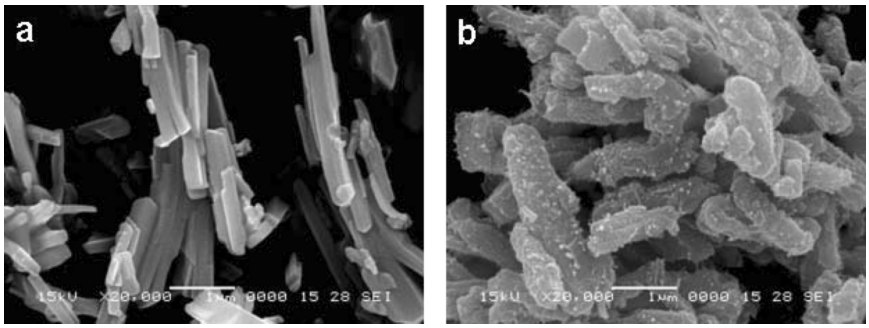

Fig. 1. SEM images of (a) $K_2Ti_4O_9$ and (b) PANI/$K_2Ti_4O_9$ composite.

line is homogeneously polymerized on the surface of the $K_2Ti_4O_9$ particles, which forms the composite with core-shell structure shown in Figure 1b.

Figure 2 gives the XRD patterns of $K_2Ti_4O_9$, PANI and PANI/ $K_2Ti_4O_9$ composites. In the pattern of PANI sample, two well-resolved peaks at ~20.8 and 25.5° are assigned to the periodicity parallel and perpendicular to the polymer chain, indicating that doped PANI is in semi-crystalline phase (28). It can also be noted that the diffraction pattern of PANI/$K_2Ti_4O_9$ is similar to that of pure $K_2Ti_4O_9$ except that the peak intensity of the composites decreases in comparison with that of $K_2Ti_4O_9$. This phenomenon indicates that the deposition of PANI on the surface of $K_2Ti_4O_9$ particles has no influence on the crystal structure of $K_2Ti_4O_9$, whereas the addition of $K_2Ti_4O_9$ results in a decrease in the degree of crystallinity and the diffraction peaks of PANI in the composite accordingly weaken gradually (29).

The structural changes caused by deposition of PANI on $K_2Ti_4O_9$ particles were followed through FTIR spectra (Figure 3). The spectrum of pure PANI (curve c) exhibits the characteristic bands in the 1000–1600 cm^{-1}. For example, the C=C stretching deformation of the quinoid (1560 cm^{-1}) and benzenoid rings (1480 cm^{-1}), the C–N stretching mode for the benzenoid ring (1300 cm^{-1}) and the C=N stretching vibrations at about 1230 cm^{-1} are observed, which is in good agreement with the emeraldine salt form of polyaniline (30). Similar bands are also visible in the composite (curve b), which suggest that PANI has been formed in the composite.

To estimate the amount of deposited PANI on the $K_2Ti_4O_9$ particles, the samples were analyzed by TGA. Figure 4 presents the TGA curves of $K_2Ti_4O_9$, PANI and PANI/$K_2Ti_4O_9$ composite. Curve (a) reveals that pure $K_2Ti_4O_9$ is relatively stable in air and only slight decomposition is observed in the range of 25–800°C. As for PANI/$K_2Ti_4O_9$ and PANI (curve b and c), they show a two-step weight loss. The first weight loss at the lower temperature results from the residual water, dopant molecules and unreacted monomer. The second weight loss at the higher temperature is due to the structural decomposition of polymer chains. Apparently, the degradation of polymer in the pure PANI and PANI/$K_2Ti_4O_9$ composite starts

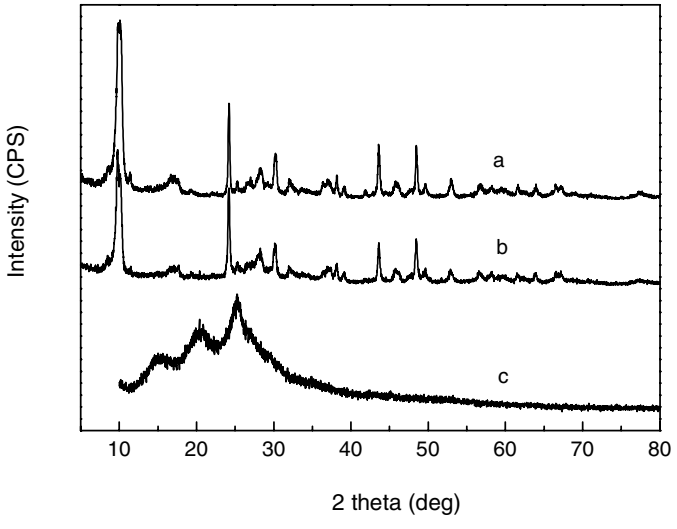

Fig. 2. XRD patterns of (a) $K_2Ti_4O_9$, (b) PANI/$K_2Ti_4O_9$ and (c) PANI.

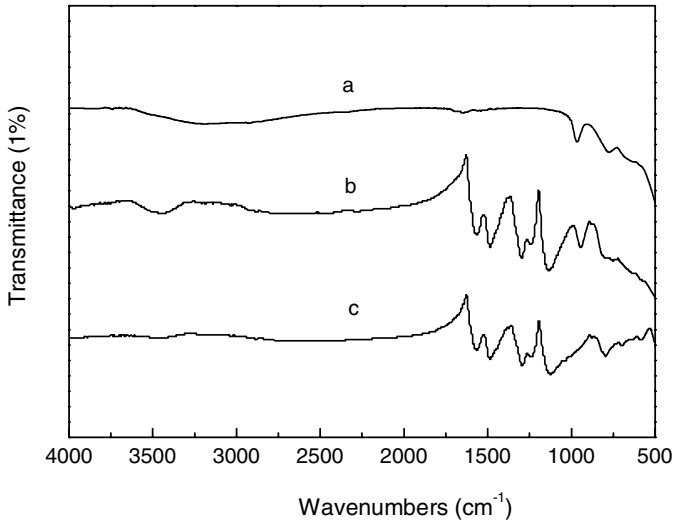

Fig. 3. FTIR spectra of (a) $K_2Ti_4O_9$, (b) PANI/$K_2Ti_4O_9$ and (c) PANI.

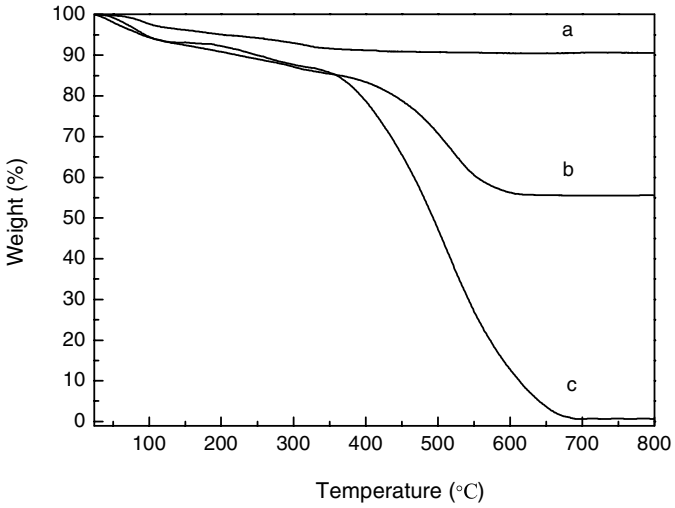

Fig. 4. TG curves of (a) $K_2Ti_4O_9$, (b) PANI/$K_2Ti_4O_9$ and (c) PANI.

at around 352 and 403°C, respectively, indicating that the composite exhibits better stability than the pure PANI. Furthermore, in comparison with curve (b) and (c), the amount of PANI in the composite is estimated to be 28.7%.

3.2 Electrorheological Properties

Figure 5 presents the typical flow curves for PANI/$K_2Ti_4O_9$ suspension under steady shear. Without an electric field, the suspension shows slight departure from the Newtonian fluid. When an electric field is applied, the shear stress increases abruptly with electric field strength and the flow curves become considerably pseudoplastic. Under an external electric field, the PANI/$K_2Ti_4O_9$ particles in the suspension are polarized to form chain- or column-like structure aligned along the field direction. As a shear field is applied, the chains or columns will suffer from deformations or destructions. In the low shear rate region, the electrostatic forces induced by the applied electric field are dominant over hydrodynamic forces induce by the external flow field (31), so the suspension shows solid-like behavior and exhibits a much larger shear stress increase under an applied electric field. While in the high shear rate region, the chain-like structures are destroyed and the hydrodynamic forces rather than electrostatic polarization start to dominate the flow behavior, thus the shear stress approaches the field-off value with increasing shear rate. On the other hand, the change of the microstructure of PANI/$K_2Ti_4O_9$ fluid results in a significant decrease in the viscosity, i.e., strong shear thinning behavior of the fluid is clearly observed as shown in Figure 6.

Figure 7 shows the dependence of the static yield stress on the electric field strength for PANI/$K_2Ti_4O_9$ composite suspension. The yield stress (τ_y) increases with increasing electric field strength (E), and the correlation between τ_y and E can be described as $\tau_y \propto E^{\alpha}$. In general, the exponent of α is predicted to be 2 from the classic polarization model (32). However, in our study the value of α is calculated to be approximately 1.46 if all the data in Figure 7 are fitted to a single straight line, which deviates from the theoretical prediction ($\alpha = 2$). This difference is mainly caused by several factors, such as particle concentration, shape of the particle, the range of the electric field strength and nonlinear conductivity of oil (33). This similarly nonlinear ER behavior ($\tau_y \propto E^{\alpha}$, $\alpha < 2$) has also been reported for various conducting polymer based ER fluids (7,15,34).

To further investigate the change of the microstructure of the PANI/$K_2Ti_4O_9$ based fluid, dynamic tests by an oscillatory shear were also performed to study the viscoelastic properties of the solidified ER fluid under an

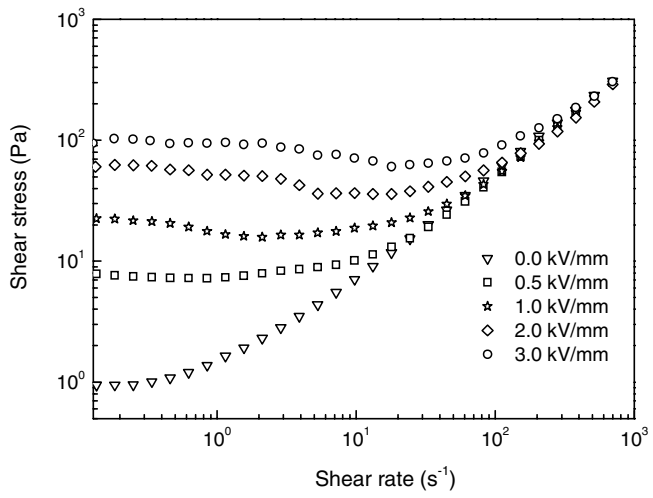

Fig. 5. Shear stress as a function of shear rate for PANI/$K_2Ti_4O_9$ fluid under different electric field strengths.

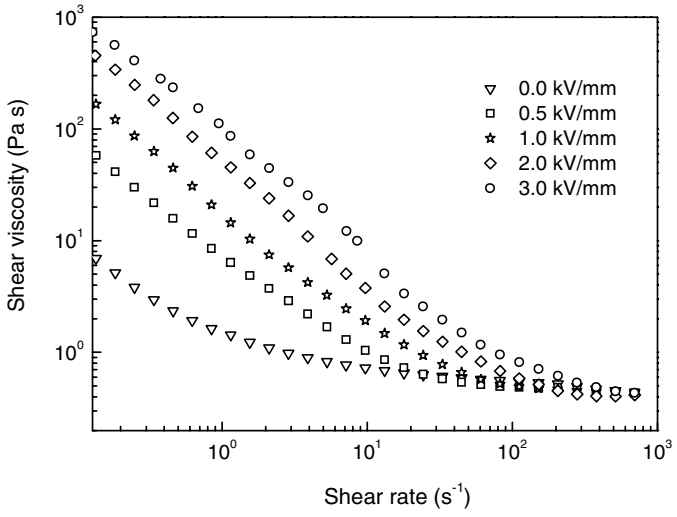

Fig. 6. Shear viscosity as a function of shear rate for PANI/$K_2Ti_4O_9$ fluid under different electric field strengths.

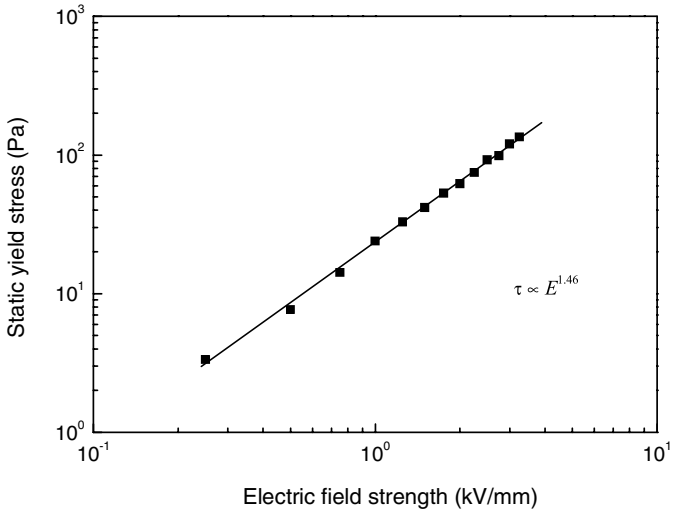

Fig. 7. Static yield stress vs. electric field strength for PANI/$K_2Ti_4O_9$ fluid.

applied electric field. Figure 8 shows the storage modulus (G') and loss modulus (G'') as a function of strain for PANI/$K_2Ti_4O_9$ suspension under various electric field. In the absence of an electric field, G'' dominates over G' indicating that the suspension shows liquid-like behavior. When an electric field is applied to the suspension, both moduli increase with electric field strength over the entire range of strain. For example, G' increases by around four orders of magnitude as the electric field strength is increased up to 3.0 kV/mm. Meanwhile, in the linear viscoelastic region, G' is larger than G''. This phenomenon is related to the elasticity of the ER fluid, which originates from column-like structures formed by polarized PANI/$K_2Ti_4O_9$ particles induced by an imposed electric field. In the linear viscoelastic region, with increasing electric field the particle chain structures become more elastic and stiffer to sustain the larger strain and the elasticity is dominant in contrast with the viscosity (i.e.,$G' > G''$). When the strain is increased gradually, the chain-like structures experience continuous destruction and reconstruction. Finally, the structures collapse beyond the critical strain demonstrating the viscous behavior (i.e., $G'' > G'$) (21).

In addition, the effect of frequency on G' and G'' for PANI/$K_2Ti_4O_9$ based fluid is also investigated as depicted in Figure 9. At zero field, both moduli are dependent of frequency, namely increase with frequency, and G'' is larger than G'. On application of an electric field, G' and G'' increase significantly with the electric field strength over a wide range of frequency. However, it is worth noting that G' keeps almost constant at higher electric field as the deformation frequency is up to 100 rad/s., i.e., G' become independent of frequency at low frequency region. An increase in electric field strength induces a higher dipole moment, which results in thicker chains spanning the two electrodes. The thicker chains in turn give rise to more elasticity of the suspension (35), as revealed by an increase of G' regardless of frequency.

The change in the microstructure of chains formed by PANI/$K_2Ti_4O_9$ particles can also be observed directly by optical microscopy. Figure 10 presents optical microscope images of the formation of chains of PANI/$K_2Ti_4O_9$ particles in silicone oil under an applied electric field. Without an electric field, the particles are randomly dispersed in silicone oil between two electrodes. When an electric field is applied (e.g. $E = 2.0$ kV/mm), the particles form dense chains or columns within one second, and the structure remains stable as long as the field is applied (right of Fig. 10). The dense chains or columns make the suspension strongly

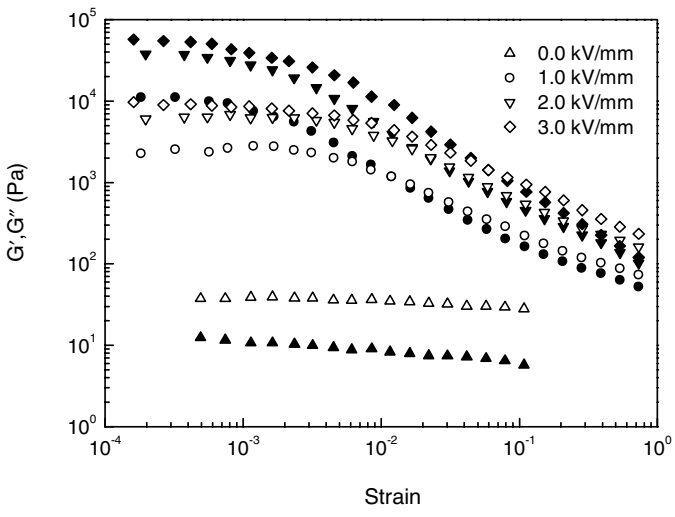

Fig. 8. G' and G'' as a function of strain for PANI/$K_2Ti_4O_9$ fluid under different electric field strengths: solid symbols for G', open symbols for G''.

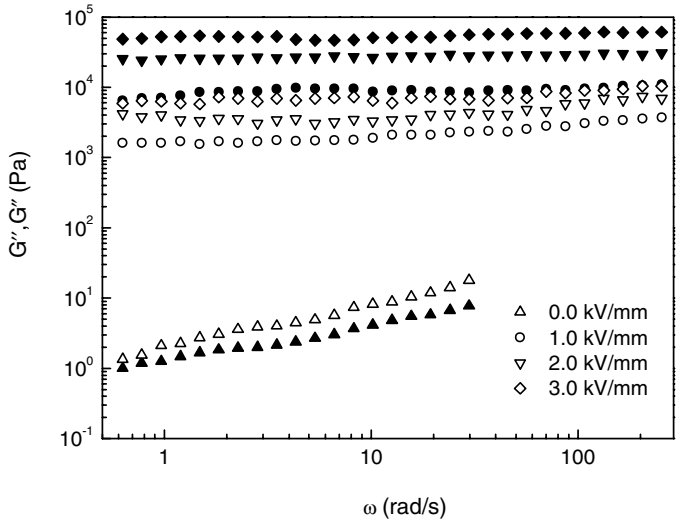

Fig. 9. G' and G'' as a function of angular frequency for PANI/$K_2Ti_4O_9$ fluid under different electric field strengths: solid symbols for G', open symbols for G''.

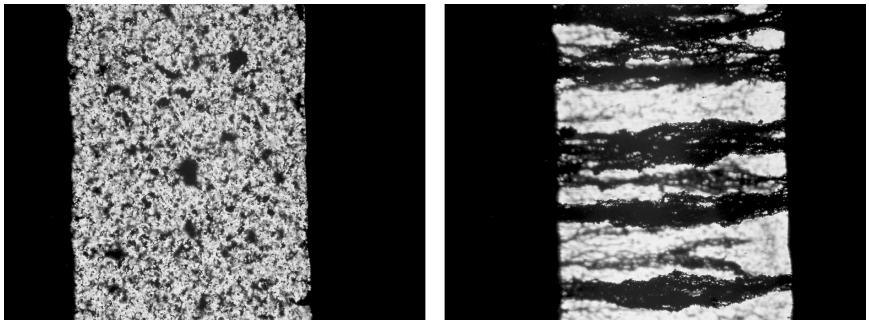

Fig. 10. Optical microscope images of 2 wt% PANI/$K_2Ti_4O_9$ particles dispersed in silicone oil placed between two electrodes before (left) and after applying electric field (2 kV/mm) (right).

solidified, which results in more elasticity of the suspension with increasing electric field strength.

4 Conclusions

In this study, the polyaniline/$K_2Ti_4O_9$ composite with core-shell structure was synthesized via chemical oxidative polymerization of aniline in the presence of silane-modified $K_2Ti_4O_9$ particles. The characterization of the prepared composite confirmed that polyaniline was deposited on the surface of $K_2Ti_4O_9$ particles, and the composite showed better thermal stability compared to pure polyaniline. It was found that the suspension of polyaniline/$K_2Ti_4O_9$ exhibited typical ER behavior under an external electric field. The measured yield stress was proportional to $E^{1.46}$ following the nonlinear conduction model. The microstructure of the composite particles based fluid became stiffer with the electric field strength, which led to higher G' and G''.

References

1. Lu, X., Ly, J., Han, S., Zhang, D., Requicha, A., Thompson, M.E. and Zhou, C. (2005) *Adv. Mater.*, 17, 2727–2732.
2. Jang, J., Nam, Y. and Yoon, H. (2005) *Adv. Mater.*, 17, 1382–1386.
3. Bissessur, R. and White, W. (2006) *Mater. Chem. Phys.*, 99, 214–219.
4. Sahoo, N.G., Jung, Y.C., So, H.H. and Cho, J.W. (2007) *Synthetic Met*., 157, 374–379.
5. Li, X., Wan, M., Wei, Y., Shen, J. and Chen, Z. (2006) *J. Phys. Chem. B*, 110, 14623–14626.
6. Bhat, S.V. and Vivekchand, S.R.C. (2006) *Chem. Phys. Lett.*, 433, 154–158.
7. Cheng, Q., Pavlinek, V., Lengalova, A., Li, C., He, Y. and Saha, P. (2006) *Micropor. Mesopor. Mater.*, 93, 263–269.
8. Kim, J.W., Liu, F., Choi, H.J., Hong, S.H. and Joo, J. (2003) *Polymer*, 44, 289–293.
9. Lengalova, A., Pavlinek, V., Saha, P., Stejskal, J. and Quadrat, O. (2003) *J. Colloid Interf. Sci.*, 258, 174–178.
10. Gao, Z. and Zhao, X.. (2003) *Polymer*, 44, 4519–4526.
11. Hao, T. (2001) *Adv. Mater.*, 13, 1847–1856.
12. Yin, J.B. and Zhao, X.P. (2006) *J. Phys. Chem. B*, 110, 12916–12925.
13. Wang, B.X. and Zhao, X.P. (2005) *Langmuir*, 21, 6553–6559.
14. Cho, M.S., Cho, Y.H., Choi, H.J. and Jhon, M.S. (2003) *Langmuir*, 19, 5875–5881.
15. Kim, Y.D. and Park, D.H. (2002) *Colloid Polym. Sci.,* 280, 828–834.
16. Chotpattananont, D., Sirivat, A. and Jamieson, A.M. (2006) *Polymer*, 47, 3568–3575.
17. Eristi, C., Yavuz, M., Yilmaz, H., Sari, B. and Unal, H.I. (2007) *J. Macromol. Sci. Part A: Pure Appl. Chem.*, 44, 759–767.
18. Wang, B.X. and Zhao, X.P. (2005) *Adv. Funct. Mater*., 15, 1815–1820.
19. Fang, F.F., Sung, J.H. and Choi, H.J. (2006) *J. Macromol. Sci. Part B: Phys.*, 45, 923–932.
20. Cheng, Q., Pavlinek, V., Lengalova, A., Li, C., Belza, T. and Saha, P. (2006) *Micropor. Mesopor. Mater.*, 94, 193–199.
21. Cho, M.S., Choi, H.J. and Ahn, W.S. (2004) *Langmuir*, 20, 202–207.
22. Park, S.J., Park, S.Y., Cho, M.S., Choi, H.J. and Jhon, M.S. (2005) *Synthetic Met.*, 152, 337–340.
23. Yin, J.B. and Zhao, X.P. (2008) *Colloid Surf. A*, 329, 153–160.
24. Liu, Y.C., Huang, J.M., Tsai, C.E., Chuang, T.C. and Wang, C.C. (2004) *Chem. Phys. Lett.*, 387, 155–159.
25. Cheng, Q., Pavlinek, V., He, Y., Li, C., Lengalova, A. and Saha, P. (2007) *Eur. Polym.* J., 43, 3780–3786.
26. Cheng, Q., He, Y., Pavlinek, V., Li, C. and Saha, P. (2008) *Synthetic Met*. 158, 953–957.
27. Ide, Y. and Ogawa, M. (2006) *J. Colloid Interf. Sci*., 296, 141–149.
28. Pouget, J.P., Jozefowicz, M.E., Epstein, A.J., Tang, X. and MacDiarmid. A.G. (1991) *Macromolecules*, 24, 779–789.
29. Xia, H. and Wang, Q. (2002) *Chem. Mater.*, 14, 2158–2165.
30. Li, C.C. and Zhang, Z.K. (2004) *Macromolecules*, 37, 2683–2685.
31. Woo, D.J., Suh, M.H., Shin, E.S., Lee, C.W. and Lee, S.H. (2005) *J. Colloid Interf. Sci.*, 288, 71–74.
32. Klingenberg, D.J., Vanswol, F. and Zukoski, C.F. (1991) *J. Chem. Phys.*, 94, 6170–6178.
33. Davis, L.C. (1997) *J. Appl. Phys*., 81, 1985–1991.
34. Kim, Y.D. and Kim, J.H. (2008) *Synthetic Met*., 158, 479–483.
35. Hiamtup, P., Sirivat, A. and Jamieson, A.M. (2006) *J. Colloid Interf. Sci.*, 295, 270–278.